The Astrophysical Journal Letters, 892:L35 (5pp), 2020 April 1 https://doi.org/10.3847/2041-8213/ab8228
© 2020. The American Astronomical Society. All rights reserved.

A 1201 s Orbital Period Detached Binary: The First Double Helium Core White Dwarf LISA Verification Binary

Warren R. Brown[1], Mukremin Kilic[2], A. Bédard[3], Alekzander Kosakowski[2], and P. Bergeron[3]
[1] Smithsonian Astrophysical Observatory, 60 Garden Street, Cambridge, MA 02138, USA
[2] Homer L. Dodge Department of Physics and Astronomy, University of Oklahoma, 440 West Brooks Street, Norman, OK 73019, USA
[3] Département de Physique, Université de Montréal, C.P. 6128, Succ. Centre-Ville, Montréal, Quebec H3C 3J7, Canada
Received 2020 February 7; revised 2020 March 18; accepted 2020 March 19; published 2020 April 6

Abstract

We report the discovery of a 1201 s orbital period binary, the third shortest-period detached binary known. Sloan Digital Sky Survey J232230.20 + 050942.06 contains two He-core white dwarfs orbiting with a 27° inclination. Located 0.76 kpc from the Sun, the binary has an estimated Laser Interferometer Space Antenna (LISA) 4 yr signal-to-noise ratio of 40. J2322 + 0509 is the first He + He white dwarf LISA verification binary, a source class that is predicted to account for one-third of resolved LISA ultra-compact binary detections.

Unified Astronomy Thesaurus concepts: Compact binary stars (283); DA stars (348); DC stars (0); Gravitational wave sources (677); Gravitational waves (678); White dwarf stars (1799); Compact objects (288); Detached binary stars (375)

Supporting material: data behind figure

1. Introduction

White dwarf (WD) binaries promise to be among the most scientifically rich "multi-messenger" sources that can be observed with both light and gravitational waves (GWs). ESA and NASA are building a space-based GW observatory called the Laser Interferometer Space Antenna (LISA; Amaro-Seoane et al. 2017) that will measure mHz GW frequencies. Astrophysically, this is the realm of <1 hr orbital period double-degenerate binaries. WD + WD binaries are expected to be the most prolific LISA source (Nelemans et al. 2001; Korol et al. 2017). Importantly, WDs emit light and we can observe them now.

Here, we report the discovery of the 1201 s orbital period binary SDSS J232230.20 + 050942.06 (hereafter J2322 + 0509). This is the third shortest-period detached binary after J0651 + 2844 (Brown et al. 2011) and ZTF J1539 + 5027 (Burdge et al. 2019a). While similar in period to J0935 + 4411 (Kilic et al. 2014) and PTF J0533 + 0209 (Burdge et al. 2019b), J2322 + 0509 has a face-on orientation $i = 27°$. It has no detectable light curve or binary astrometric signal; only time-series spectroscopy is able to detect its period.

We combine spectroscopy, photometry, and astrometry to characterize the system. J2322 + 0509 is a single-lined spectroscopic binary with a 19,000 K WD moving with a velocity semi-amplitude of $k = 149\,\mathrm{km\,s^{-1}}$. Multi-passband photometry shows that a cooler companion contributes an additional 15% extra light at red wavelengths. Astrometry sets an absolute distance to the system, and places a direct constraint on the WD radii. We perform a joint analysis and conclude that J2322 + 0509 is an approximately equal-mass, double-degenerate binary containing a 0.27 $M_\odot$ DA WD and a 0.24 $M_\odot$ DC WD.

J2322 + 0509 is thus the first double He-core (He + He) WD LISA verification binary. Models predict this source class will account for about one-third of resolved LISA ultra-compact binary detections (Lamberts et al. 2019). LISA will detect J2322 + 0509 with an estimated signal-to-noise ratio (S/N) $\simeq$ 40 in 4 yr of operation.

2. Observations

We targeted J2322 + 0509 on the basis of its Gaia parallax and Sloan Digital Sky Survey (SDSS) colors. Following the release of Gaia Data Release 2 (DR2; Gaia Collaboration et al. 2018), we searched the Gaia catalog for extremely low-mass WD candidates that might be missing from the ELM Survey (Brown et al. 2020). We selected candidates with de-reddened SDSS color $-0.40 < (g - r)_0 < -0.10$ mag (approximately $20,000 > T_{\rm eff} > 10,000$ K) and with Gaia parallax consistent with a $\sim$0.1 $R_\odot$ low-mass WD. J2322 + 0509, at the blue edge of the sample, is an interesting result. We present our observations followed by our analysis. Measured and derived values are summarized in Table 1.

2.1. Spectroscopy

We obtained an exploratory spectrum of J2322 + 0509 on UT 2018 December 9 to determine its stellar nature. We used the Blue Channel spectrograph on the 6.5 m MMT telescope with the 832 $1\,\mathrm{mm^{-1}}$ grating in second order, giving 1.0 Å resolution. J2322 + 0509 has the hydrogen Balmer line spectrum of a DA WD. We fit pure hydrogen stellar atmosphere models (Gianninas et al. 2011, 2014, 2015) and determined that J2322 + 0509 is a $\log g \simeq 7$ WD. WDs with such gravities are commonly found in ultra-compact binaries, because the universe is not old enough to evolve a low-mass WD through single-star evolution (e.g., Iben 1990; Marsh et al. 1995).

The following year we obtained time-series MMT Blue Channel spectroscopy to test for binary orbital motion. We observed low-amplitude radial velocity variability, but were unable to determine a period until we took back-to-back exposures on UT 2019 October 5. On UT 2019 October 8, we observed J2322 + 0509 with a lower 2.0 Å resolution set-up, using the MMT Blue Channel 800 $1\,\mathrm{mm^{-1}}$ grating, so that we could better time-resolve the orbital period (150 s = 1/8 orbital phase) at the cost of lower velocity precision. Figure 1 plots the measurements.

Table 1
J2322 + 0509 System Parameters

Parameter	Value
Astrometric (Gaia DR2)	
R.A. (J2000)	23:22:30.203
Decl. (J2000)	+5:09:42.061
Plx (mas)	1.287 ± 0.283
$\mu_{\rm R.A.}$ (mas yr^{-1})	11.094 ± 0.428
$\mu_{\rm decl.}$ (mas yr^{-1})	−7.119 ± 0.336
Photometric (SDSS DR14)	
u (mag)	18.853 ± 0.028
g (mag)	18.589 ± 0.018
r (mag)	18.906 ± 0.015
$E(B-V)$ (mag)	0.062
Spectroscopic (MMT + Magellan)	
P (s)	1201.4 ± 5.9
k (km s^{-1})	148.6 ± 6.3
γ (km s^{-1})	−4.8 ± 4.2
T_0 BJD$_{\rm TDB}$ (d)	2458764.685470 ± 0.000228
$T_{\rm eff,DA,spec}$ (K)	19160 ± 270
$\log g_{\rm DA,spec}$ (cm s^{-2})	7.17 ± 0.04
Joint Analysis (Adopted)	
$d_{\rm plx}$ (kpc)	0.76 ± 0.17
$T_{\rm eff,DA}$ (K)	19000 ± 1000
$\log g_{\rm DA}$ (cm s^{-2})	7.0 ± 0.15
$T_{\rm eff,DC}$ (K)	8000 ± 1500
$\log g_{\rm DC}$ (cm s^{-2})	7.0 ± 0.25
Derived	
$M_{\rm DA}$ ($M_\odot$)	$0.27^{+0.06}_{-0.02}$
$M_{\rm DC}$ ($M_\odot$)	$0.24^{+0.06}_{-0.04}$
a ($R_\odot$)	0.194 ± 0.007
i (deg)	27.0 ± 3.8

Finally, on UT 2019 November 20, we obtained 1 hr of MagE spectroscopy on the 6.5 m Magellan Baade telescope to test for spectral lines from a companion in the red end of the spectrum. We used the 0.″85 slit and 180 s exposures. We confirmed the radial velocity parameters of the primary WD, but phase-folding the spectra reveals no evidence of spectral lines from the secondary WD.

2.2. Photometry

We obtained time-series photometry of J2322 + 0509 using the 8 m Gemini North telescope with the Gemini Multi-Object Spectrograph on UT 2019 October 24 as part of the Director's Discretionary Time program GN-2019B-DD-201. We obtained 170 × 10 s exposures through an SDSS-g filter over 84 minutes. To reduce the read-out time, we binned the chip by 4 × 4, which resulted in a plate scale of 0.″3 pixel^{-1}. Conditions were photometric with 0.″5 seeing. Figure 2 shows the light curve and its Fourier transform.

We observe no significant variability at the 4 $\langle A \rangle$ = 3.8 millimag (0.35%) level. Interestingly, the highest peak in the Fourier transform—3.1 ± 0.9 millimag amplitude at 69 ± 3 cycles day^{-1}—is consistent with the radial velocity period, however it is only marginally significant. The predicted amplitude of the relativistic beaming effect is only 0.1% (Shporer et al. 2010), below our detection threshold. No eclipses or ellipsoidal variation are detected.

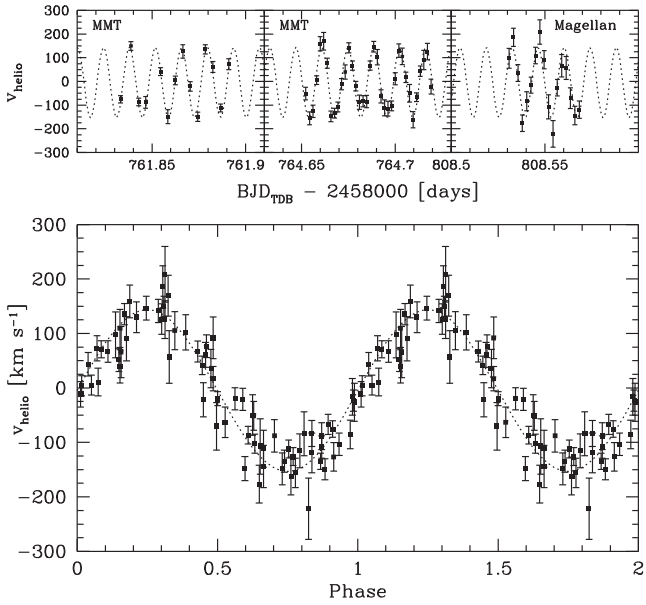

Figure 1. Radial velocities phased to the best-fit orbital solution. (The data used to create this figure are available.)

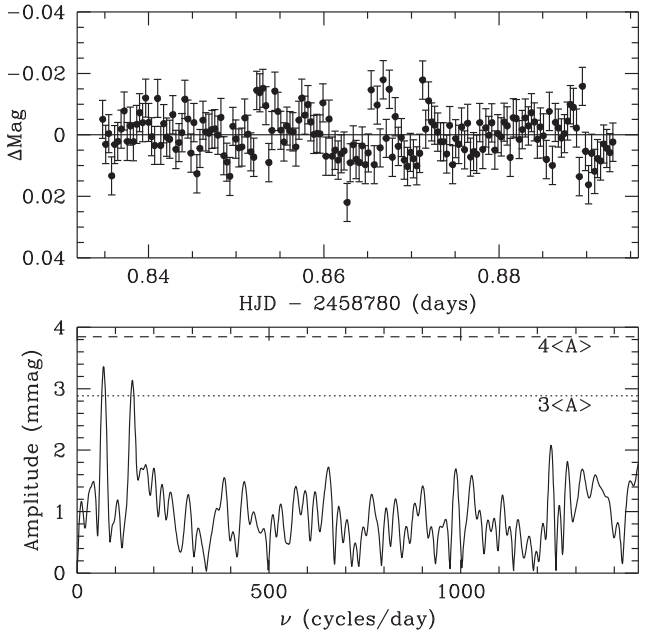

Figure 2. Optical light curve (top panel) and its Fourier transform (bottom panel). The absence of variability above $4 < A > = 0.35\%$ sets an upper limit on inclination $i < 50°$.

3. Analysis

J2322 + 0509 is a single-lined spectroscopic binary. We solve for its radial velocity orbital parameters following the same procedure used in previous ELM Survey papers (Brown et al. 2020). We start by cross-correlating the full spectra with a summed, rest-frame template of the target. Comparing the independent MMT and Magellan data sets suggests our zero-point accuracy is 2 km s^{-1}. We then minimize χ^2 for a circular orbit solution, accounting for phase smearing given the exposure times. We estimate internal uncertainties by bootstrap re-sampling the measurements. The best-fit radial velocity

solution of the combined MMT and Magellan data sets is $P = 1201.4 \pm 5.9$ s, $k = 148.6 \pm 6.3$ km s^{-1}, and $\gamma = -4.8 \pm 4.2$ km s^{-1} (see Figure 1).

We fit pure hydrogen (DA WD) stellar atmosphere models to the summed, rest-frame MMT, and Magellan spectra. The $T_{\rm eff}$ and log$g$ values from the independent MMT and Magellan data sets are consistent within their errors. The weighted mean values are $T_{\rm eff,spec} = 19160 \pm 270$ K, $\log g_{\rm spec} = 7.17 \pm 0.04$ dex.

High-order Balmer lines are sensitive to surface gravity (Tremblay & Bergeron 2009) and allow us to constrain the DA WD mass given a WD mass–radius relation. We adopt the He-core WD models of Althaus et al. (2013) appropriate for this object. Interpolating the stellar atmosphere values with their errors through the models yields $M_{\rm DA,spec} = 0.34 \pm 0.02\ M_\odot$. The corresponding g-band absolute magnitude, $+9.27 \pm 0.18$ mag, allows us to compute its heliocentric distance if the light of the DA WD dominates the light of the (de-reddened) $g_0 = 18.351 \pm 0.018$ mag binary.

However, we find evidence for additional light from the companion star in the broadband spectral energy distribution. If we normalize the DA WD model to the SDSS u-band magnitude, the g- and r-bands are 15% ± 2% too bright. Accounting for this excess g-band light, our spectroscopic parameters imply the DA WD is $d_{\rm spec} = 0.72 \pm 0.07$ kpc distant.

Gaia parallax provides an independent but less precise measure of heliocentric distance. Adopting the Gaia DR2 parallax zero-point of −0.029 mas (Lindegren et al. 2018), J2322 + 0509's 1.287 ± 0.283 mas parallax corresponds to $d_{\rm plx} = 0.76 \pm 0.17$ kpc. The spectroscopic and parallax distances are in perfect agreement.

The absence of a significant reflection effect constrains the orientation of the binary. We use JKTEBOP (Southworth et al. 2004) to create synthetic light curves for the adopted system parameters below. JKTEBOP predicts peak-to-peak differences of >1% for inclinations >50°. Given that no significant photometric signal is detected above the 0.35% level, we can safely rule out such high inclinations. If we instead use Equation (6) from Morris & Naftilan (1993) to predict the amplitude of the reflection effect, we find that the inclination must be $i < 58°$. Hence, both light curve modeling and analytic estimates require $i \lesssim 50°$otherwise we would see a reflection effect.

3.1. Joint Analysis

We now perform a joint analysis that considers our spectroscopic, astrometric, and photometric constraints simultaneously. Our approach is to construct composite binary models by adding two synthetic WD spectra, properly weighted by their respective radii using the astrometric parallax constraint. We then simultaneously fit the spectroscopic Balmer line profiles and the broadband photometric measurements using the Levenberg–Marquardt algorithm (Bédard et al. 2017; Kilic et al. 2020). We use de-reddened Galaxy Evolution Explorer far-ultraviolet (FUV) and near-ultraviolet (NUV; Martin et al. 2005), SDSS *ugriz* (Abolfathi et al. 2018), Pan-STARRS *grizy* (Tonry et al. 2012), and UKIDSS *YJ* photometry (Lawrence et al. 2007). All four atmospheric parameters ($T_{\rm eff,1}$, $\log g_1$, $T_{\rm eff,2}$, and $\log g_2$) are allowed to vary for a given distance.

Figure 3 plots the best-fit solution: a 19,000 K DA WD plus a 8000 K DC WD, both with log$g = 7$. We note that a DA + DA solution yields comparable parameters, but predicts a strong double-lined Hα feature that is not observed. The errors in the joint analysis are dominated by the parallax uncertainty. We estimate 1σ errors of 1000 K in $T_{\rm eff}$ and 0.15 dex in $\log g$ for the DA WD, and 1500 K in $T_{\rm eff}$ and 0.25 dex in $\log g$ for the DC WD.

We interpolate the atmospheric parameters through the Althaus et al. (2013) He-core WD tracks to estimate the masses. Conservatively ignoring the co-variance between $T_{\rm eff}$ and $\log g$, we infer $M_{\rm DA,joint} = 0.27^{+0.06}_{-0.02}\ M_\odot$ and $M_{\rm DC,joint} = 0.24^{+0.06}_{-0.04}\ M_\odot$.

Our mass estimates imply that the cool WD may be less massive than the hot WD. The same result is seen in ZTF J1539 + 5027 (Burdge et al. 2019a). This would be surprising because one expects the cool WD to have evolved first, and thus be more massive than the hot WD. However the models contain a major uncertainty linked to common envelope ejection (Li et al. 2019, 2020). The thickness of the WD hydrogen envelope, assumptions about elemental diffusion and rotational mixing, the presence or absence of hydrogen shell flashes, and other issues have significant effects on the temperature, radius, and cooling age of a low-mass WD (Althaus et al. 2013; Istrate et al. 2016). To draw a significant conclusion about the WD masses and their past evolution, we need to improve our constraints, i.e., with future GW measurements. The present constraints are also consistent with J2322 + 0509 being an equal-mass binary.

Given the mass estimates, we predict that J2322 + 0509's orbital period is shrinking by $\dot{P} = -2.2 \times 10^{-12}$ s s^{-1} due to GW radiation. Measuring $\dot{P}$ is challenging in the absence of a timing signal from eclipses. However, the phase of the radial velocity orbit also provides a means to measure $\dot{P}$. We simulate radial velocity data to estimate the timing constraints. At the MMT, times are recorded using network time protocol accurate to milliseconds, and open-shutter time is accurate to ∼0.1 s. Our current data set has a ±20 s epoch error. Simulations suggest that 6 contiguous hours on-source (4 times our best baseline) with current measurement errors would achieve a ±10 s epoch error in a single night.

We expect J2322 + 0509's orbital phase to shift by 91 s in 10 yr, and by 364 s in 20 yr when LISA is observing. With ±10 s epoch errors and every-other-year observations, we could attain a 5σ measurement of $\dot{P}$ in 14 yr. The two WDs will merge due to GW radiation in $6.7^{+2.8}_{-1.8}$ Myr.

4. Discussion

J2322 + 0509 is a new GW source for LISA to observe. While the GW community may refer to J2322 + 0509 as a verification binary, optical measurements are critical to its scientific understanding. LISA will continuously monitor the entire sky; Shah et al. (2013) estimated that simply knowing a binary's sky position can improve its GW parameter uncertainties by a factor of two. GW strain depends on binary inclination; having an inclination constraint can improve the GW parameter uncertainties by a factor of 40 (Shah et al. 2013).

Solving the binary mass function for inclination,

$$\sin i = k\left(\frac{P}{2\pi G}\right)^{1/3}\frac{(M_1 + M_2)^{2/3}}{M_2}, \quad (1)$$

our optical measurements of orbital period, velocity semi-amplitude, and mass constrain J2322 + 0509's inclination to

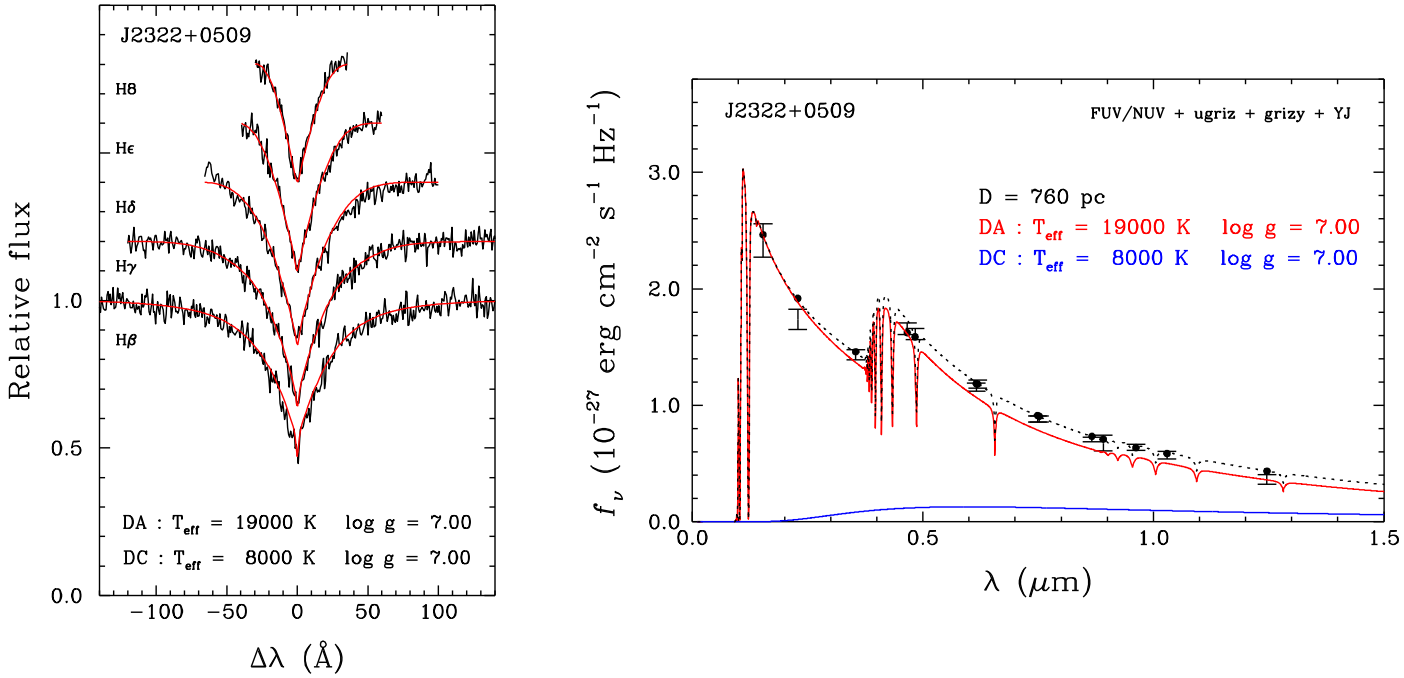

Figure 3. Joint fit to the spectrum (left panel) and photometry (right panel) for the best DA + DC model. The left panel shows the synthetic model (red) overplotted on the observed MMT spectrum (black). The right panel shows the synthetic fluxes (filled circles) and observed fluxes (error bars). The red and blue lines show the contribution of each WD to the total monochromatic model flux, displayed as the black dotted line.

$i = 27.0 \pm 3.8$ deg. This inclination results in a 2.5 times larger GW strain than if J2322 + 0509 had $i = 90°$ and were eclipsing.

Figure 4 plots the characteristic strain of J2322 + 0509 relative to the 4 yr LISA sensitivity curve (Robson et al. 2019). Solid diamonds are detached WD binaries from the ELM Survey (Brown et al. 2020), and open diamonds are the two detached WD binaries found by Burdge et al. (2019a, 2019b). We calculate strain using spectroscopic distance estimates for the sake of consistency, and label only those binaries significantly above the 4 yr LISA sensitivity curve.

J2322 + 0509 has a larger strain than the signature verification binaries J0651 + 2844 and J1539 + 5027, because it is closer and orientated face-on. However J2322 + 0509 will be detected at lower S/N because of its lower frequency $f_{\rm GW} = 2/P = 1.66$ mHz. According to the LISA Detectability Calculator, J2322 + 0509 is predicted to have a 4 yr S/N ≃40 (Q. S. Baghi 2020, private communication). The same estimator yields S/N = 154 for J0651 + 2844 ($M_1 = 0.25\ M_\odot$, $M_2 = 0.5\ M_\odot$, $d = 1$ kpc, $P = 765$ s, $i = 86°$) as a point of reference.

Binary population synthesis models predict that most LISA sources will be found in the Galactic disk (Breivik et al. 2019; Lamberts et al. 2019). J2322 + 0509 fits that picture. Combining J2322 + 0509's Gaia parallax and proper motion with our radial velocity, corrected for the 6.6 ± 0.9 km s^{-1} gravitational redshift of the DA WD, yields a space motion $(U, V, W) = (-36.1 \pm 8.0, -20.4 \pm 4.6, -3.8 \pm 4.4)$ km s^{-1} with respect to the Sun. J2322 + 0509 is located 0.6 kpc below the Galactic plane but clearly has the motion of a disk star.

Interestingly, J2322 + 0509 is the first He + He WD system among the LISA verification binaries. Population synthesis models predict that 30% of resolved LISA systems will be He + He binaries, 50% will be He + CO binaries, and 20% will be CO + CO binaries (Lamberts et al. 2019).

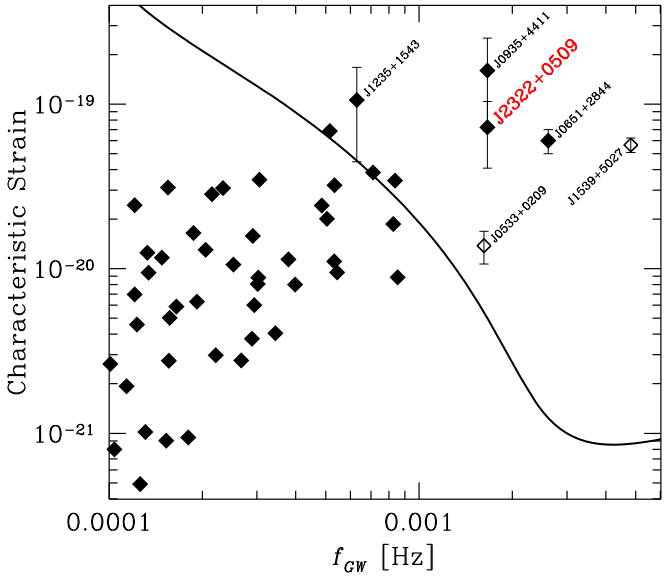

Figure 4. Characteristic strain vs. GW frequency for J2322 + 0509 and other detached WD binaries from Brown et al. (2020; solid diamonds) and Burdge et al. (2019a, 2019b; open diamonds). The solid line is the LISA 4 yr sensitivity curve (Robson et al. 2019).

Observationally, all of the detached binaries with $f > 1$ mHz are He + CO WD binaries, except for J2322 + 0509.

Future GW measurements promise to improve our understanding of the WD binary systems. For J1539 + 5027, Littenberg & Cornish (2019) estimated that GW measurements will improve its inclination uncertainty by a factor of 5 and its distance uncertainty by a factor of 10. Similar improvements in mass and orbital evolution open the door to new tests, for example measuring tidal dissipation in WDs (Fuller & Lai 2012, 2013; Piro 2019). In order to have the time baseline

to measure parameters like $\dot{P}$, it is important to continue finding future multi-messenger systems like J2322 + 0509 now.

We thank A. Milone and Y. Beletsky for their assistance with observations obtained at the MMT and Magellan telescopes, respectively. This research makes use the SAO/NASA Astrophysics Data System Bibliographic Service. This work was supported in part by the Smithsonian Institution, the NSF under grant AST-1906379, the NSERC Canada, and by the Fund FRQ-NT (Québec).

Based on observations obtained at the Gemini Observatory, which is operated by the Association of Universities for Research in Astronomy, Inc., under a cooperative agreement with the NSF on behalf of the Gemini partnership: the National Science Foundation (United States), National Research Council (Canada), CONICYT (Chile), Ministerio de Ciencia, Tecnología e Innovación Productiva (Argentina), Ministério da Ciência, Tecnologia e Inovação (Brazil), and Korea Astronomy and Space Science Institute (Republic of Korea).

Facilities: MMT (Blue Channel spectrograph), Magellan:Clay (MagE spectrograph), Gemini:North (GMOS spectrograph).

Software: IRAF (Tody 1986, 1993), RVSAO (Kurtz & Mink 1998), JKTEBOP (Southworth et al. 2004).

ORCID iDs

Warren R. Brown https://orcid.org/0000-0002-4462-2341
Mukremin Kilic https://orcid.org/0000-0001-6098-2235
A. Bédard https://orcid.org/0000-0002-2384-1326
Alekzander Kosakowski https://orcid.org/0000-0002-9878-1647
P. Bergeron https://orcid.org/0000-0003-2368-345X

References

Abolfathi, B., Aguado, D. S., Aguilar, G., et al. 2018, ApJS, 235, 42
Althaus, L. G., Miller Bertolami, M. M., & Córsico, A. H. 2013, A&A, 557, A19
Amaro-Seoane, P., Audley, H., Babak, S., et al. 2017, arXiv:1702.00786
Bédard, A., Bergeron, P., & Fontaine, G. 2017, ApJ, 848, 11
Breivik, K., Coughlin, S. C., Zevin, M., et al. 2019, ApJ, submitted, arXiv:1911.00903
Brown, W. R., Kilic, M., Hermes, J. J., et al. 2011, ApJL, 737, L23
Brown, W. R., Kilic, M., Kosakowski, A., et al. 2020, ApJ, 889, 49
Burdge, K. B., Coughlin, M. W., Fuller, J., et al. 2019a, Natur, 571, 528
Burdge, K. B., Fuller, J., Phinney, E. S., et al. 2019b, ApJL, 886, L12
Fuller, J., & Lai, D. 2012, MNRAS, 421, 426
Fuller, J., & Lai, D. 2013, MNRAS, 430, 274
Gaia Collaboration, Brown, A. G. A., Vallenari, A., et al. 2018, A&A, 616, A1
Gianninas, A., Bergeron, P., & Ruiz, M. T. 2011, ApJ, 743, 138
Gianninas, A., Hermes, J. J., Brown, W. R., et al. 2014, ApJ, 781, 104
Gianninas, A., Kilic, M., Brown, W. R., Canton, P., & Kenyon, S. J. 2015, ApJ, 812, 167
Iben, I., Jr. 1990, ApJ, 353, 215
Istrate, A. G., Marchant, P., Tauris, T. M., et al. 2016, A&A, 595, A35
Kilic, M., Bédard, A., Bergeron, P., & Kosakowski, A. 2020, MNRAS, 493, 2805
Kilic, M., Brown, W. R., Gianninas, A., et al. 2014, MNRAS, 444, L1
Korol, V., Rossi, E. M., Groot, P. J., et al. 2017, MNRAS, 470, 1894
Kurtz, M. J., & Mink, D. J. 1998, PASP, 110, 934
Lamberts, A., Blunt, S., Littenberg, T., et al. 2019, MNRAS, 490, 5888
Lawrence, A., Warren, S. J., Almaini, O., et al. 2007, MNRAS, 379, 1599
Li, Z., Chen, X., Chen, H.-L., et al. 2020, ApJ, in press (arXiv:2003.02480)
Li, Z., Chen, X., Chen, H.-L., & Han, Z. 2019, ApJ, 871, 148
Lindegren, L., Hernandez, J., Bombrun, A., et al. 2018, A&A, 616, A2
Littenberg, T. B., & Cornish, N. J. 2019, ApJL, 881, L43
Marsh, T. R., Dhillon, V. S., & Duck, S. R. 1995, MNRAS, 275, 828
Martin, D. C., Fanson, J., Schiminovich, D., et al. 2005, ApJL, 619, L1
Morris, S. L., & Naftilan, S. A. 1993, ApJ, 419, 344
Nelemans, G., Yungelson, L. R., Portegies Zwart, S. F., & Verbunt, F. 2001, A&A, 365, 491
Piro, A. L. 2019, ApJL, 885, L2
Robson, T., Cornish, N. J., & Liu, C. 2019, CQGra, 36, 105011
Shah, S., Nelemans, G., & van der Sluys, M. 2013, A&A, 553, A82
Shporer, A., Kaplan, D. L., Steinfadt, J. D. R., et al. 2010, ApJL, 725, L200
Southworth, J., Maxted, P. F. L., & Smalley, B. 2004, MNRAS, 351, 1277
Tody, D. 1986, Proc. SPIE, 627, 733
Tody, D. 1993, in ASP Conf. Ser. Vol. 52, Astronomical Data Analysis Software and Systems II, ed. R. J. Hanisch, R. J. V. Brissenden, & J. Barnes (San Francisco, CA: ASP), 173
Tonry, J. L., Stubbs, C. W., Lykke, K. R., et al. 2012, ApJ, 750, 99
Tremblay, P.-E., & Bergeron, P. 2009, ApJ, 696, 1755